Photocatalytic activity of Al/Ni-doped TiO2 films synthesized by sol-gel method: Effect of sunlight photocatalysis on the catalysts properties

Elhachmi Guettaf Temam (elhachemi.guettaf@univ-biskra.dz)
Universite Mohamed Khider de Biskra https://orcid.org/0000-0001-6868-7484

Faiçal Djani
Universite Mohamed Khider de Biskra Faculte des Sciences Exactes et des Sciences de la Nature et de la Vie

Saad Rahmane
Universite Mohamed Khider de Biskra Faculte des Sciences Exactes et des Sciences de la Nature et de la Vie

Hachemi Ben Temam
Universite Mohamed Khider de Biskra Faculte des Sciences et de la Technologie

Brahim Gasmi
Universite Mohamed Khider de Biskra Faculte des Sciences et de la Technologie

Research Article

Keywords: Al, Ni doped TiO2, Thin films, Sol gel, Methylene blue, Photocatalysis, Sunlight

Posted Date: February 16th, 2021

DOI: https://doi.org/10.21203/rs.3.rs-211595/v1

Photocatalytic activity of Al/Ni-doped TiO_2 films synthesized by sol-gel method: Effect of sunlight photocatalysis on the catalysts properties

Elhachmi Guettaf Temam[1], Faiçal Djani[2], Saad Rahmane[1], Hachemi Ben Temam[1], Brahim Gasmi[1]*

[1] *Physics Laboratory of Thin Layers and Applications, Biskra University, BP 145 RP, Biskra 07000, Algeria*

[2] *Molecular Chemistry Laboratory and Environment, University Mohamed Khider, 07000 Biskra, Algeria*

* Corresponding author: elhachemi.guettaf@univ-biskra.dz (Elhachmi Guettaf Temam)

Tel: +213 661 273 182

Abstract

Photocatalytic activity of semiconductors is affected by the nature of metal dopant. To study the effect of non-transition and transition metal on the physical and optical properties of TiO_2 based photocatalysts; Al and Ni-doped TiO_2 thin films respectively were prepared via a sol-gel dip-coating method. The effect of the photocatalysis process on the properties of TiO_2 based thin films was investigated. The photocatalytic activity was calculated from methylene blue dye degradation under sunlight irradiation. XRD results show that un-doped TiO2 films were grown with anatase phase, whereas, the Ni and Ni/Al-doped TiO_2 films show Ti_4O_7 single phase. The presence of Al preferred the rutile phase. No phases related to NiO or Al_2O_3 were detected. Ni-TiO2 photocatalyst shows high photocatalytic activity (~93%) thanks to the high content of O and Ti, wide bandgap (3.35 eV), low crystal size (6.87 nm), high film thickness (288 nm), and high surface roughness (44.5 nm). After photocatalysis, all the films show a decrease in O content and thickness, whereas the indirect bandgap values were increased which suggesting the reuse with low photocatalytic activity.

Keywords:

Al, Ni doped TiO_2; Thin films; Sol gel; Methylene blue; Photocatalysis; Sunlight.

1. Introduction

Titanium dioxide TiO_2 is a versatile transition-metal oxide that has a large number of applications such as protective coatings [1-2], Photodetector [3], optical thin films [4-5], microelectronic devices [6], self-cleaning [7-9], and photocatalyst for the breakdown of organic contaminants in wastewaters [10-13]. All these applications are a traduction of their attractive properties such as high transmission in the visible region, wide band gap for anatase phase (3.4 eV), and high photocatalytic activity under UV light [14].

As well known, there is two technologic ways for the illumination of organic substances from wastewater by the heterogeneous photocatalytic processes, i.e. suspended and fixed type. The suspended photocatalyst has more active surface sites than the fixed one due to its movement and nature of the material used (powder); however, its separation from treated solution is an issue [15]. The fixed photocatalyst has an advantage to mostly employ as thin films that are easy to use on an industrial scale at low cost.

In recent years, variety of researches have involved studying the photocatalytic properties of TiO_2 thin films exposed under sunlight [16-18] and UV light radiations [19-21]. Wen et al. [22] studied the effect of doping TiO_2 catalyst by I and F on the degradation rate of methylene blue and disclosed that TiO_2 photocatalyst exhibited much higher activity under UV light than that under simulated sunlight. Yu et al. [23] reported that the photocatalytic activity of TiO_2 thin film was remarkably enhanced by Ni doping at 0.5 at. % dopant concentration. The general mechanism of TiO_2 semiconductor photocatalysis is described step by step in the literature [24, 25].

In this study, we purposed a cost-effective solution within the fields of wastewater treatment before putting it up. Aluminum and Nickel doped TiO_2 photocatalyst thin films were synthesized on glass substrates by sol-gel dip-coating technique and then characterized. Al and Ni are chosen as non-transition and transition metal respectively, to study the effect of metal doped TiO_2 thin films on the photodegradation rate of methylene blue dye under sunlight irradiation.

2. Experimental details

2.1. Materials

All chemicals were used as received from Sigma Aldrich without any purification. Double distilled water was used for all experiments. Sol-gel dip coating technique was used for the synthesis of Al/Ni/TiO_2 thin films. Titanium (IV) isopropoxide [$Ti(OCH(CH_3)_2)_4$], Nickel (II) nitrate hexahydrate [$Ni(NO_3)_2.6H_2O$], and Aluminum nitrate nonahydrate [$Al(NO_3)_3.9H_2O$] were used as the precursor materials for TiO_2, Ni, and Al respectively. Water, isopropanol and ethanol were functioned as solvents. Glacial acetic acid was used as a chelating agent.

2.2. Titanium dioxide-Ni-Al thin films synthesis

The sol has been formed by dissolving TTIP in water and isopropanol (iPrOH) then stirred for 30 min. Later, Glacial acetic acid was added dropwise into the sol with vigorous stirring for 2 h at room temperature. The molar ratio of the components was optimized at H_2O: iPrOH: TTIP: Glacial acetic acid = 2:25:1:1. The final solution is a transparent yellowish. To synthesis Al and Ni doped TiO_2 thin films, Nickel (II) nitrate hexahydrate (Ni 3 wt. %) and Aluminum nitrate nonahydrate (Al 3 wt. %) were dissolved in 10 ml ethanol for 60 min and then added to the previous solution respectively.

Glass substrates were cleaned in acetone for 5 min to avoid any organic contamination and then washed with ethanol and water. The substrates were dipped in the prepared solutions for 30 seconds, and then withdrawn at a speed of 0.8 $mm.s^{-1}$ and dried at 100 °C for 5 min to evaporate organic solvents. The dip-coating procedure was repeated five times. All the TiO_2 based thin films were calcined at 450 °C for 3 hours.

2.3. Al/Ni/TiO_2 thin films caracterization

The crystallographic structure of the films was evaluated by X-ray diffraction using a Bruker diffractometer (D8 Advance model) with CuKa radiation (λ=1.5406 Å), scanning from 20–80° at a rate of 0.03° s^{-1}. The 3D surface topography and the surface roughness of the films were analyzed by mechanical profilometer (Tencor P-7). The surface morphology of Al/Ni/TiO_2 films was studied using (JEOL JSM 5800) scanning electron microscope (SEM) coupled with an energy dispersive X-ray analyzer (EDX) to study the chemical composition of the photocatalysts. The optical transmission spectra of the films were conducted with a UV-VIS JASCO V-770 spectrophotometer at a wavelength from 300-1500 nm.

2.4. Photocatalytic caracterization

The photocatalytic experiments by exploiting sunlight irradiation were conducted on the 15th of December 2020, under the conditions of the weather for that day (Biskra-Algeria). We intended to mention the date, as both the mean air temperature and relative humidity affect the solar radiation and therefore the photocatalytic efficiency of the films [26-30]. In addition, we aim for an in-depth study to compare the photocatalytic performance of TiO_2 based thin films under sunlight irradiation every 15th of each month.

In this study, Methylene blue (MB) dye has chosen as a model of wastewater contaminants. Photocatalytic degradation of MB solutions by TiO_2 based thin films was investigated under sunlight irradiation. The photocatalyst samples (20 cm^2) were dipped in 100 ml of MB solution (2ppm), in a Pyrex beaker at an angle of 36 ° ± 1 with tracking the direction of the sun manually during the experiments as an imitation of the solar panel system. Before the reaction, the photocatalyst was kept in the MB solution in the dark for 30 min to reach adsorption equilibrium, and then the irradiation tests were carried out from 8:30 am to 3:30 pm. During these experiments, the MB solution has stirred with a speed of 250 rpm.

3. Results & discussion

3.1. TiO_2 based thin films properties

Figure 1 shows the XRD patterns of Al/Ni/TiO_2 thin films. The XRD pattern of pure TiO_2 exhibits a tetragonal crystal structure with a single anatase phase (A) at the diffraction line 25.4° (JCPDS: 00-002-0387); this result is similar to a previous study [31]. The Ni-TiO_2 film reveals that Ni doping TiO_2 produced a change in the crystalline structure from anatase to anorthic structure of Ti_4O_7 phase [32] with diffraction line 31.7° (JCPDS: 00-018-1402). The XRD result of Al-TiO_2 thin film shows two peaks at 38.4

and 44.2 ° corresponding to the Ti_3O_5 (Monoclinic, JCPDS: 00-011-0217) and rutile (Tetragonal, JCPDS: 00-003-1122) phase, respectively. The Al-Ni-TiO_2 thin film reveals a similar XRD results to that of Ni-TiO_2 film. Rutile crystal phase has tighter band gap (3.0 eV) than that of anatase phase (3.4 eV) [33], therefore, it suggest low photocatalytic activity due to the recombinition of electrons from the conduction to the valence band (hole). Crystal size, porosity, and roughness of TiO_2 material are ones of important factors influencing its catalytic activity. Choi et al. [34] disclosed that small crystal size is of importance for high photocatalytic activity of TiO_2 material. The primary crystal size was valued based on the effective crystal dimension *D* computed using Scherrer equation which is given in the form

$$D = 0.9 \cdot \frac{\lambda}{B \cdot cos\theta} \quad (1)$$

Where 0.9 is the Scherrer constant, λ is the wavelength of X-ray (1.5406 Å), *B* is the full wave half-maximum, and θ is the Bragg angle [35]. *D* values were calculated for the most intense diffraction line (Table 1). The crystal size of TiO_2 based thin films was around 6-9 nm. Based on the literature [36, 37], Ni-TiO_2 catalyst promises high photocatalytic efficiency compared to other catalysts as it has small particle size (6.87 nm). Moreover, Ni and Al doping decrease the crystal size due to the incorporation of Ni^{2+} and Al^{3+} ions into cation sites of TiO_2 lattice.

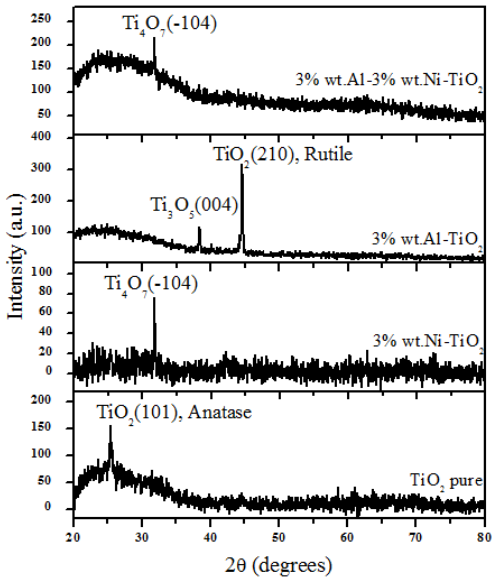

Fig. 1. XRD patterns of TiO_2 based thin films.

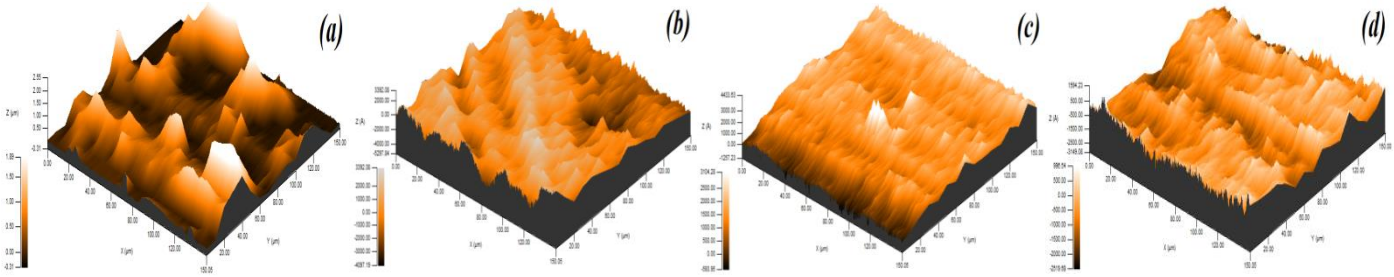

Fig. 2. 3D surface topography of TiO_2 based thin films: (a) TiO_2 pure, (b) 3 wt. %Ni-TiO_2, (c) 3 wt. %Al-TiO_2, (d) 3 wt. %Ni-3 wt. %Al-TiO_2.

The 3D surface topography of un-doped TiO_2 and Al/Ni doped TiO_2 thin films is shown in Fig. 2. The root mean square (R_q) surface roughness was calculated with the use of Apex analysis software (Table 1). The surface of TiO_2 thin film is heterogeneous with a height equal to 1890 nm. This surface is modified by the presence of Ni which makes the surface porous and flat with a certain difference in the density of pores dispersed randomly. Al doping TiO_2 films makes the surface homogenous. The height of Al/Ni/TiO_2 thin films is between 1.5-4.5 nm. R_q values are in the range of 30-45 nm (Table 1). Ni-TiO_2 thin films suggest high photocatalytic efficiency for the discoloration of MB as it shows the high roughness value 44.5 nm [38]. Al-TiO_2 thin films have shown the lowest roughness 22.8 nm due to its homogenous surface.

Table. 1. Summary of analytical data

		Thin films			
		TiO_2	**Ni/TiO_2**	**Al/TiO_2**	**Al/Ni/TiO_2**
Parameters	**Units**				
Crystallographic Phase	---	(A)	Ti_4O_7	(R)	Ti_4O_7
Crystal Size	nm	8.38	6.87	7.58	6.97
Surface Roughness	nm	30.7	44.5	22.8	31,7
Film Thickness	nm	316	288	284	292
Transmission in Visible Range	%	~93	~88	~82	~85
Optical Indirect Band Gap	eV	3.41	3.35	3.32	3.26
Si Content	wt%	35.8	25.23	19.27	32.74
O Content	wt%	59.06	58.09	58.00	48.11
Ti Content	wt%	11.14	15.63	20.88	16.50
Ni Content	wt%	--	1.06	--	1.12
Al Content	wt%	--	--	1.85	1.53
photocatalytic efficiency	%	~84	~93	~64	~86
Rate constat	h^{-1}	0.224	0.428	0.159	0.320

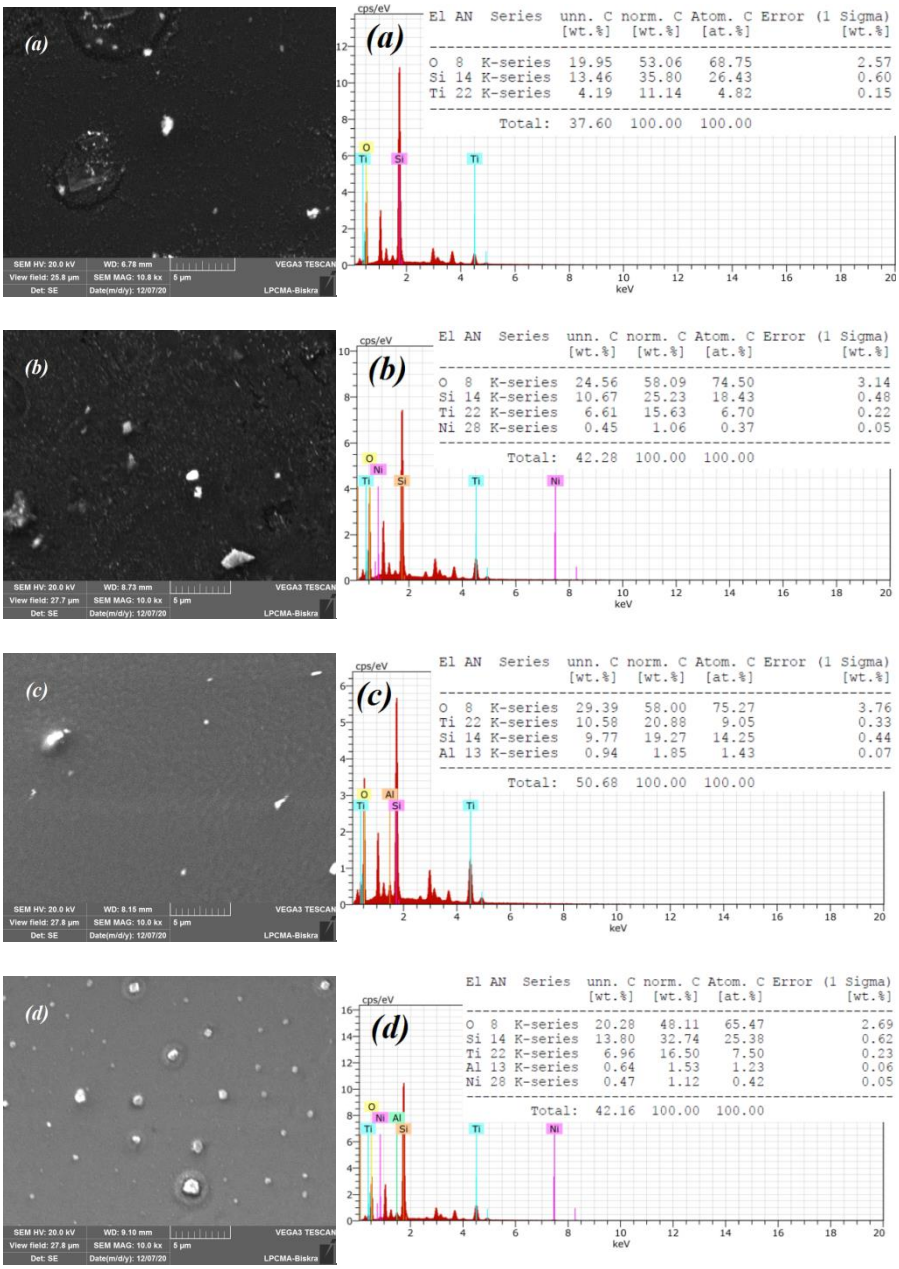

Fig. 3. SEM and EDX analyses of TiO_2 based thin films: (a) TiO_2 pure, (b) 3 wt. %Ni-TiO_2, (c) 3 wt. %Al-TiO_2, (d) 3 wt. %Ni-3 wt. %Al-TiO_2.

SEM images of TiO_2 based thin films show compact and uniform films as shown in Fig. 3. For Ni-TiO_2 thin films, it can be observed the presence of randomly distributed grains and pores which can increase the amount of MB adsorbed on these surfaces, and consequently, increasing the photocatalytic efficiency of the film. EDX analyses show a difference of the oxygen content in TiO_2 based thin films. The increase in oxygen content in thin films increases its transmittance and thus giving high band gap energy (Eg) value [33]. The O content in TiO_2 thin films is in the range 48-59 wt. % as shown in Fig. 3. Ni-TiO_2 thin film shows the higher value of O content (58.09 wt. %). Al/Ni doped TiO_2 thin films exhibits Ni and Al contents less than 2 wt. % (Table 1). The thickness (t) of TiO_2 based thin films was estimated by the gravimetric method using the relation

$$t = \frac{M}{g.A} \quad (2)$$

Where t is the films thickness (cm), A is the surface area of the films (cm^2), M is the mass of the films (g), and g is the density of the film material ($g.cm^{-3}$) [39]. Table 1 shows that films thickness values confirm the 3D film growth as shown in Fig. 2. TiO_2 films with the best high (1980 nm) and much high crystal size (8.38 nm) is the thickest film. The doping of TiO_2 films by Ni and Al reduce the thickness of the films to 288 nm and 284 nm, respectively.

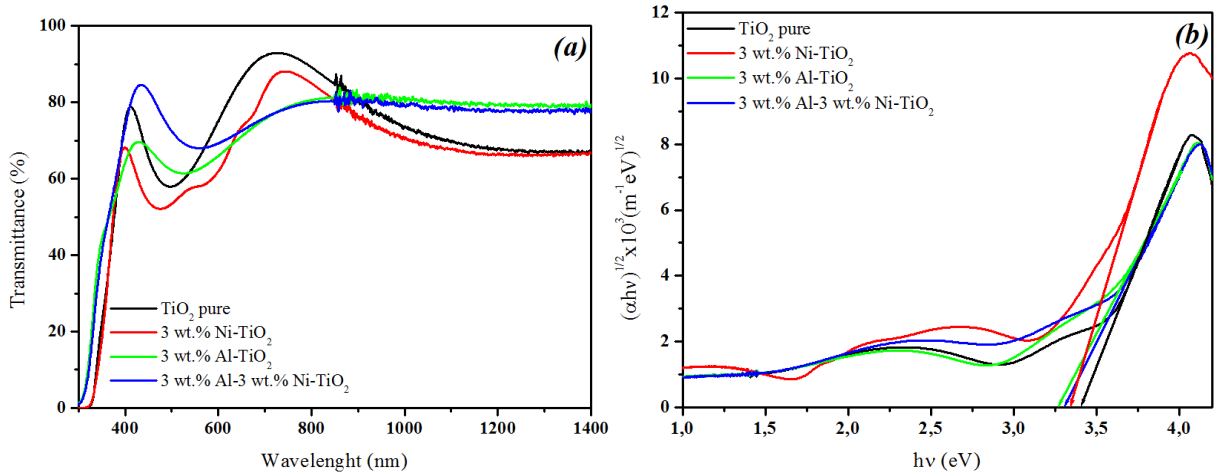

Fig. 4. (a) UV-VIS optical transmission spectra of TiO_2 based thin films,

(b) Tauc plot for the optical band gap.

Figure 4 shows the optical transmission spectra of the films and Tauc plot for the optical band gap (Eg). The transmission spectra show high transparency in the visible region for all the TiO_2 based thin films. These films have a transmittance values greater than 80%. The highest transmittance value is for TiO_2 pure with a high film thickness and oxygen content: 316 nm and 59.06 wt. %, respectively. It is tempting to conclude that the average transmittance is a function of film thickness and oxygen content with a proportional relationship (Table1). The optical indirect band gap was estimated using Tauc and Menth method given by relation (eq. 3)

$$(\alpha h\nu)^{1/2} = C(h\nu - E_g) \quad (3)$$

$$\alpha = \frac{1}{t}\ln\left(\frac{T}{100}\right) \quad (4)$$

Where α is the absorption coefficient (m^{-1}) (eq. 4), which should be identified by the equation 4, h is Planck's constant ($4.136*10^{-15}$ eV.s), ν is Frequency of light (s^{-1}), C is a Constant, Eg is Optical indirect band gap (eV), t is the film thickness (m) and T is the optical transmittance (%) [40]. The band gaps of the films slightly decreased with doping TiO_2 thin films by Ni and Al ions owing to the change in crystallographic phase from anatase to Ti_4O_7 and rutile, respectively. In other hand, both degree of crystallinity [19], crystal size [17] and film thickness [39] are the of importance parameters controlling the film band gap value. Table 1 shows that the indirect band gap widens with increasing thickness [41]. The wide band gap (3.41 eV) for TiO_2 thin film agrees with high crystal size (8.38 nm) and thickness (316 nm).

3.2. Photocatalytic performance

The photocatalytic performance of TiO_2 based thin films was evaluated through the photodegradation of MB in an aqueous solution under sun irradiation. Fig. 5(a) shows that MB decomposes continuously throughout the entire irradiation time for Ni-doped TiO_2 thin films. The rate of degradation varies according to the hour of irradiation, since solar radiation is affected by temperature, humidity, wind speed, etc. The photocatalytic efficiency (γ) is determined from the following equation [42]:

$$\gamma\% = \frac{(C_0 - C_t)}{C_0} \quad (5)$$

Where C_0 and C_t are the concentrations of MB dye at times t = 0 and t, respectively. The photodegradation of MB can be fitted by a pseudo-first-order reaction kinetic model [43, 44]:

$$-\ln\left(\frac{C_0}{C_t}\right) = \kappa t \quad (6)$$

Where k is the pseudo first-order rate constant (h^{-1}) and t is the irradiation time (hours). The degree of MB degradation was in the order Ni/TiO_2 > $Al/Ni/TiO_2$ > TiO_2> Al/TiO_2 as shown in Fig. 5. Al/TiO_2 (rutile phase) film shows lower photocatalytic efficiency (~64%), than that of anatase (~84%) TiO_2 film (Table 1); it is well known that rutile phase has lower photocatalytic efficiency than anatase phase due to the low indirect band gap. Wang et al [45] studied the sonocatalytic degradation of methyl orange in the presence of nanometer anatase and rutile TiO_2 powders. The compared sonocatalytic activities showed that the catalytic activity of nanometer anatase TiO_2 powder is higher than that of nanometer rutile TiO_2 powder. Ni/TiO_2 (~93%), and $Al/Ni/TiO_2$ (~86%) as sun catalysts show an effective degradation rate compared to that of anatase TiO_2 catalyst due to the low crystal size, high roughness, and crystallographic phase (Ti_4O_7) (Table 1). Roughness enhancement increases surface area of the films [46], and consequently increases the quantity of adsorbed contaminant. Hence photodegradation predominates. In addition, the modification of TiO_2 films surface by Ni^{2+} improves photocatalytic activity under sun light which can be attributed to the decreased recombination rate electron-hole pairs. As a transition metal, nickel metal is well known as it most often has remarkable catalytic properties and can form a wide variety of ionic species in a wide range of oxidation states which gives rise to variously colored complexes due to the different electronic transitions within the incomplete $3d^8$ sub-shell. The doped metal plays an effective role in charge separation by capturing electrons. Begum et al. [47] discussed that Ni ions capture the electron that left a freer hole at the valence band which increases the holes concentration and leads to migrates to surface layer by withdrawing the electrons from the surface.

K values were determined by regression analysis of lines slopes in Fig. 5(c). Table 1 shows K values which increase with irradiation time for all TiO_2 based photocatalysts. Figure 5(d) shows that the discoloration rate constant is largest with Ni doped TiO_2 due to the low crystal size and high surface roughness. Al-TiO_2 (rutile) photocatalysts shows the smallest (k) value maybe owing to the high electron recombinition rate. Eva et al. [33] reported that as rutile adsorbs $OH^{\bullet}$ more effectively than anatase, the

amount of $OH^{\bullet}$ generated on TiO_2 and diffusing to the bulk solution would be lower in rutile crystallites. This result leads to conclude that

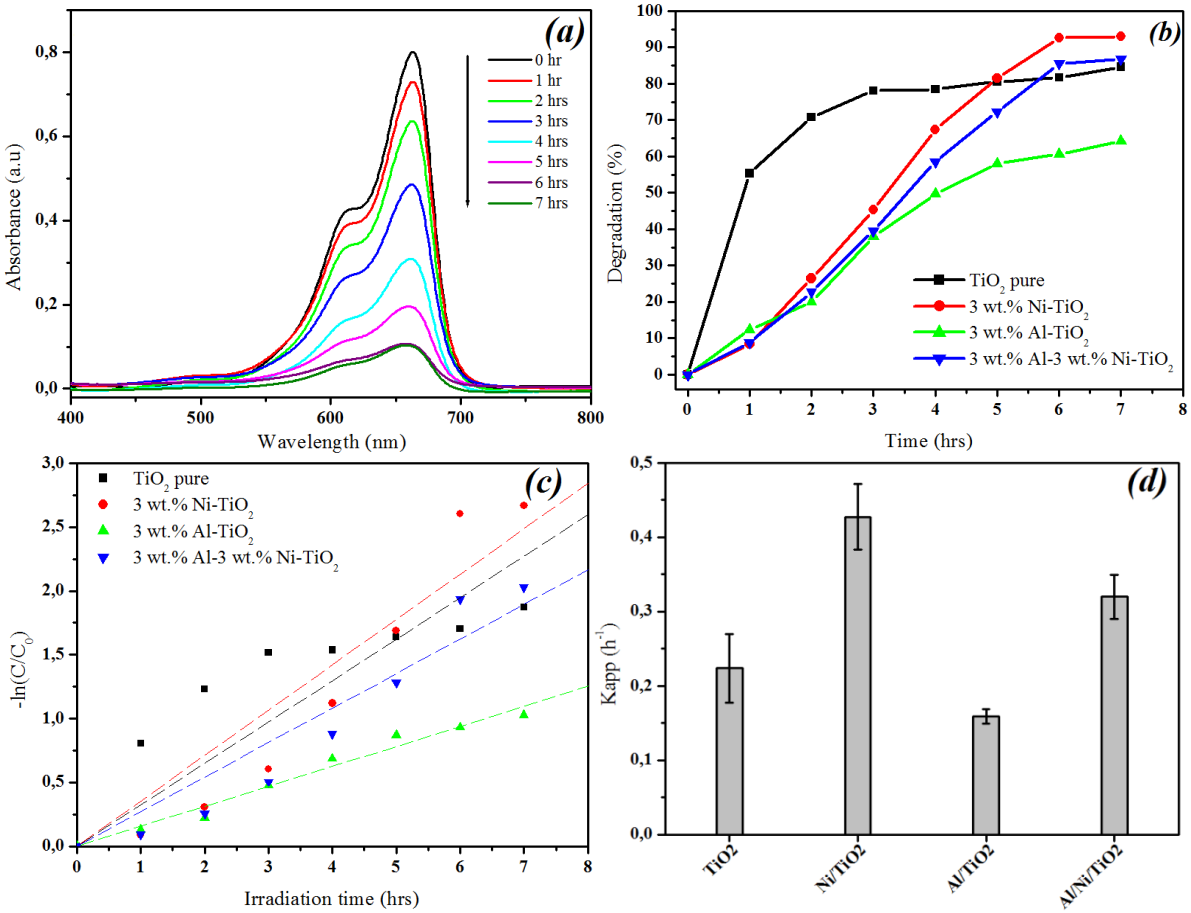

Fig. 5. (a) Variation of UV–vis spectra of MB during photodegradation over Ni/TiO_2 thin films; (b) Plot of photocatalytic efficiency versus the degradation time; (c) plot of $\ln (C/C_0)$ versus irradiation time for TiO_2 based films; (d) rate constant *k* of MB photodegradation.

the doping metal type on TiO_2 photocatalysts is of most important effective parameter on the photodegradation of MB. As discussed in above, Ni doped TiO_2 as transition metal increased the degree of photocatalysis under sunlight irradiation. In other hand, Al was chosen as non-transition metal (sub-shell: $3p^1$), which decreased the photocatalytic activity of TiO_2 thin films.

3.3. Effect of MB photodegradation process on the TiO_2 based thin films properties

Figure 6 shows surface morphology and EDX analyses of TiO_2 based thin films after photodegradation experiments under sun light irradiation. It is clear to observe that the morphology of the samples is uniform and compact compared to that before photolysis experiments; maybe owing to the high photodegradation rates of MB dye that require high photocatalytic activity of the films which leads to erode of films outer coatings. These results suppose that the thickness and surface roughness of the films are decreased by the

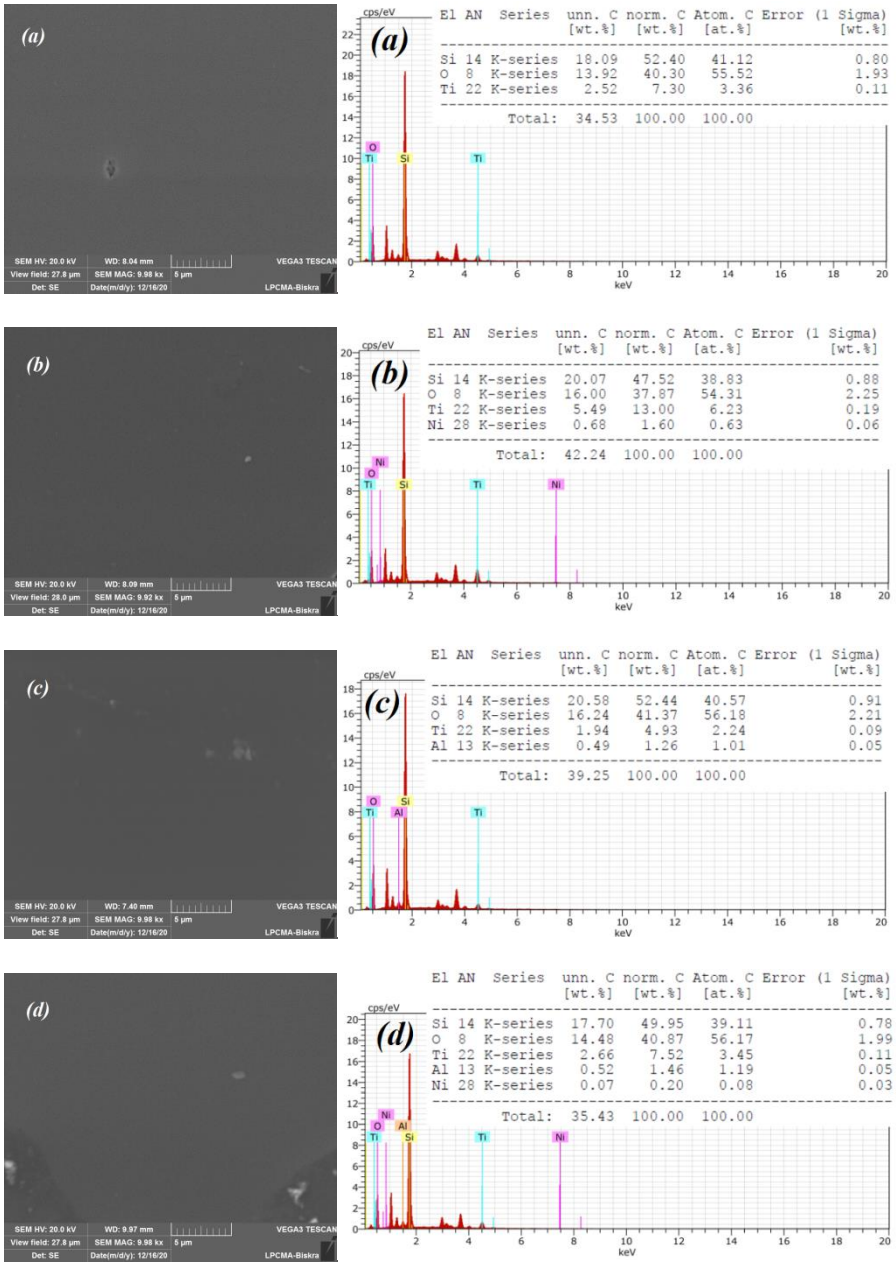

Fig. 6. SEM and EDX analyses of TiO_2 based thin films after photodegradation process: (a) TiO_2 pure, (b) 3 wt. %Ni-TiO_2, (c) 3 wt. %Al-TiO_2, (d) 3 wt. % Al-3 wt. % Ni-TiO_2.

photolysis process. Hence, it is suggesting that the reuse of these samples for second cycle of photolysis gives low photodegradation rate than the first one. EDX results show that the content of Ti and O decreased by the photocatalysis application of these films as shown in Fig. 6(b). Hoffmann et al. [24] reported that unless oxygen is supplied on a continuous basis to a photocatalytic reactor, the rate of photocatalytic oxidation will decrease dramatically after depletion of the primary electron acceptor due to charge-carrier recombination. Overall, Ti and O contents are decreased owing to the photocatalytic oxidation of MB on bulk-phase TiO_2.

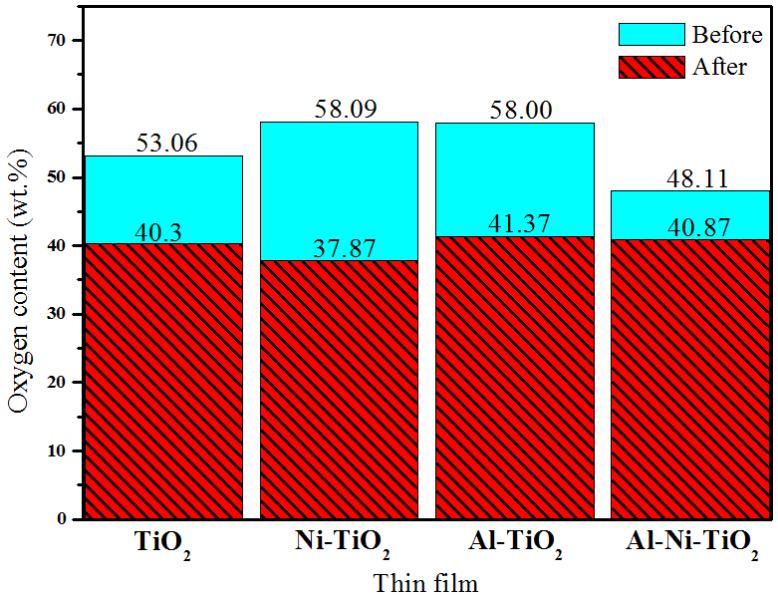

Fig. 7. Effect of photocatalysis process on oxygen content in the films.

Figure 7 shows the influence of photocatalysis process on oxygen content in the films. It is evident that the decrease in oxygen content is higher for Ni-TiO_2 films due to the high photodegradation rate as the O is the electron acceptor and the principal oxidant. The decrease in O content leads to the decreasing optical transmission.

Figure 8 shows UV-Vis transmittance spectra of TiO_2 based thin film samples and their indirect band gap after photolysis. Figure 8(a) indicates the interference fringes which imply that the films are relatively flat after sun photocatalysis experiments. Overall, the optical transmission of the films decreased with decreased films thickness by photodegradation process (Table 2). Kim et al. [48] found that the optical transmission is not exponentially related to the film thickness. This result suggests that the transmission of the TiO_2 based thin films is affected by other physical properties of the films. In this study, the transmission decreases is attributed to the decreased O content in the films by the sun photocatalysis process.

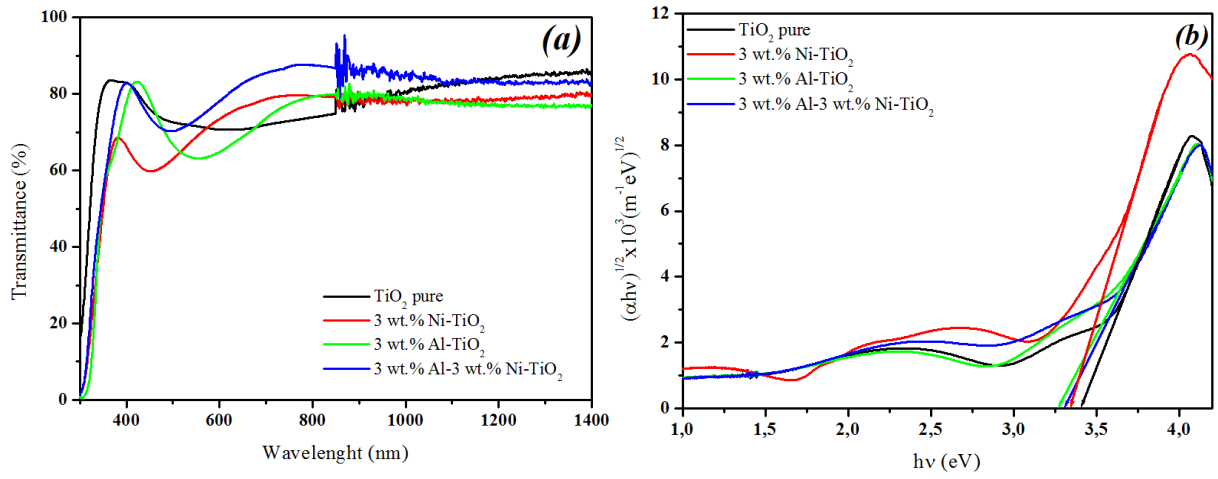

Fig. 8. (a) UV-VIS optical transmission spectra of TiO_2 based thin films after photodegradation process, (b) Tauc plot for the optical band gap.

Table. 2. Effect of photocatalysis process on the TiO_2 based thin films properties

		Thin films			
		TiO_2	Ni/TiO_2	Al/TiO_2	$Al/Ni/TiO_2$
Parameters	**Units**				
Film Thickness	nm	223	252	281	265
Transmission in Visible Range	%	~83	~80	~82	~82
Optical Indirect Band Gap	eV	3.44	3.41	3.40	3.46
Si Content	wt%	52.40	47.52	52.44	49.95
O Content	wt%	40.30	37.87	41.37	40.87
Ti Content	wt%	7.30	13.00	4.93	7.52
Ni Content	wt%	--	1.60	--	0.20
Al Content	wt%	--	--	1.26	1.46

Table 2 shows an increase in band gap with varying values according to the photocatalytic activities of the samples. This increase may lead to the low electron transfer kinetics from the valence band to the conduction band driving photo-oxidation of contaminants when using these samples for a second cycle. Trapping electron-hole of wide band gap semiconductors require high energy for photocatalysis than that of tighter one. This result suggests that using the samples for a second photocatalytic cycle may give less photodegradation rate than the first cycle. Bansode et al. [49] reused the Fe doped TiO_2 thin films for three cycles as MB bleaching photocatalysts under UV light, and found that the nature of degradation remains unaltered.

4. Conclusion

This work focused on the effect of Ni and Al dopants as transition and non-transition metal respectively, on the photocatalytic performance of TiO_2 thin films synthesized via sol-gel dip-coating technique. The photocatalytic performance of TiO_2 based thin films were evaluated via the photodegradation of methylene blue under sunlight irradiation. Photocatalysis process show that grown phase, grain size, surface morphology and roughness, O content and indirect band gap are of importance parameters controlling the photocatalytic performance of TiO_2 based thin films. 3 wt. % $Ni\text{-}TiO_2$ photocatalysts show higher degradation rate (~93%) than the other deposits. The transition metal Ni dopant improves the physical and optical properties of TiO_2 thin films. Thus the photodegradation of MB predominates. The use of 3 wt. % Al as non-transition metal dopant impairs the photocatalytic activity of TiO_2 thin films under sunlight irradiation.

Declaration of interests

The authors declare that they have no known competing financial interests or personal relationships that could have appeared to influence the work reported in this paper.

References

[1] AS Rad, Afshar A, Azadeh M (2020) Anti-reflection and self-cleaning meso porous TiO_2 coatings as solar systems protective layer: Investigation of effect of porosity and roughness. Optical Materials 107:110027.

[2] Ziadi I, Alves MM, Taryba M, El-Bassi L, Hassairi H, Bousselmi L, Montemor MF, Akrout H (2020) Microbiologically influenced corrosion mechanism of 304L stainless steel in treated urban wastewater and protective effect of silane-TiO_2 coating. Bioelectrochemistry 132:107413.

[3] Kara F, Kurban M, Coşkun B (2020) Evaluation of electronic transport and optical response of two-dimensional Fe-doped TiO_2 thin films for photodetector applications. optik 210:164605.

[4] Zarhri Z, Cardos MÁA, Ziat Y, Hammi M, ElRhazouani O, Argüello JCC, Avellaneda DA (2020) Synthesis, structural and crystal size effect on the optical properties of sprayed TiO_2 thin films: Experiment and DFT TB-mbj. Journal of Alloys and Compounds 819:153010.

[5] Salman SH, Shihab AA, Elttayef AHKh (2019) Studying The Effect of The Type of Substrate on The Structural ,Morphology and Optical Properties of TiO_2 Thin Films Prepared by RF Magnetron sputtering. Energy Procedia 157:199–207.

[6] Green ML, Schenck PK, Chang KS, Ruglovsky J, Vaudin M (2009) "Higher-κ" dielectrics for advanced silicon microelectronic devices: A combinatorial research study. Microelectronic Engineering 86:1662-1664.

[7] Adachi T, Latthe SS, Gosavi SW, Roy N, Suzuki N, Ikari H, Kato K, Katsumata KI, Nakata K, Furudate M, Inoue T, Kondo T, Yuasa M, Fujishima A, Terashima C (2018) Photocatalytic, superhydrophilic, self-cleaning TiO_2 coating on cheap, light-weight, flexible polycarbonate substrates. Applied Surface Science 458:917-923.

[8] Navabpour P, Ostovarpour S, Hampshire J, Kelly P, Verran J, Cooke K (2014) The effect of process parameters on the structure, photocatalytic and self-cleaning properties of TiO_2 and Ag-TiO_2 coatings deposited using reactive magnetron sputtering. Thin Solid Films 571:75-83.

[9] Peeters H, Keulemans M, Nuyts G, Vanmeert F, Li C, Minjauw M, Detavernier C, Bals S, Lenaerts S, Verbruggen SW (2020) Plasmonic gold-embedded TiO_2 thin films as photocatalytic self-cleaning coatings. Applied Catalysis B: Environmental 267:118654.

[10] Anis SF, Hashaikeh R, Hilal N (2019) Functional materials in desalination: A review. Desalination 468:114077.

[11] Huo P, Yan Y, Li S, Li H, Huang W (2010) Floating photocatalysts of fly-ash cenospheres supported AgCl/TiO_2 films with enhanced Rhodamine B photodecomposition activity. Desalination 256:196-200.

[12] Bouanimba N, Zouaghi R, Laid N, Sehili T (2011) Factors influencing the photocatalytic decolorization of Bromophenol blue in aqueous solution with different types of TiO_2 as photocatalysts. Desalination 275:224-230.

[13] Chen S, Cao G (2006) Study on the photocatalytic oxidation of NO_2-ions using TiO_2 beads as a photocatalyst. Desalination 194:127-134.

[14] Hamadanian M, Vanani AR, Behpour M, Esmaeily AS (2011) Synthesis and characterization of Fe, S-codoped TiO_2 nanoparticles: Application in degradation of organic water pollutants. Desalination 281:319-324.

[15] Horng RY, Huang C, Changb MC, Shao H, Shiaub BL, Hu YJ (2009) Application of TiO_2 photocatalytic oxidation and non-woven membrane filtration hybrid system for degradation of 4-chlorophenol. Desalination 245:169-182.

[16] Zahedi F, Behpour M, Ghoreishi SM, Khalilian H (2015) Photocatalytic degradation of paraquat herbicide in the presence TiO_2 nanostructure thin films under visible and sun light irradiation using continuous flow photoreactor. Solar Energy 120:287-295.

[17] Behpour M, Dehaghi RF, Mir N (2017) Considering photocatalytic activity of N/F/S-doped TiO_2 thin films in degradation of textile waste under visible and sunlight irradiation. Solar Energy 158:636-643.

[18] Li J, Hou X, Sun T, Han J, Liu H, Li D (2019) Hydrophilic, antibacterial and photocatalytic properties of TiO_2 composite films modified by the methods of N^+ ion implantation and doping of CNTs under visible light irradiation. Surface and Coatings Technology 365:123-128.

[19] Lin CP, Chen H, Nakaruk A, Koshy P, Sorrell CC (2013) Effect of Annealing Temperature on the Photocatalytic Activity of TiO_2 Thin Films. Energy Procedia 34:627-636.

[20] Velasco-Hernández A, Esparza-Muñoz RA, de Moure-Flores FJ, Santos-Cruz J, Mayén-Hernández SA (2020) Synthesis and characterization of graphene oxide - TiO_2 thin films by sol-gel for photocatalytic applications. Materials Science in Semiconductor Processing 114:105082.

[21] Rizzo L, Koch J, Belgiorno V, Anderson MA (2007) Removal of methylene blue in a photocatalytic reactor using polymethylmethacrylate supported TiO_2 nanofilm. Desalination 211:1-9.

[22] Wen C, Zhu YJ, Kanbara T, Zhu HZ, Xiao CF (2009) Effects of I and F codoped TiO_2 on the photocatalytic degradation of methylene blue. Desalination 249:621–625.

[23] Yu H, Li XJ, Zheng SJ, Xu W (2006) Photocatalytic activity of TiO_2 thin film non-uniformly doped by Ni. Materials Chemistry and Physics 97: 59-63.

[24] Hoffmann MR, Martin ST, Choi W, Bahnemannt DW (1995) Environmental Applications of Semiconductor Photocatalysis. Chem. Rev. 95:69-96.

[25] Shapovalov VI (2010) Nanopowders and Films of Titanium Oxide for Photocatalysis:A Review. Glass Physics and Chemistry 36:121–157.

[26] Hashimoto Y, Ohashi Y, Nabeshima M, Shigeta Y, Kikegawa Y, Ihara T (2019) Sensitivity of electricity consumption to air temperature, air humidity and solar radiation at the city-block scale in Osaka, Japan. Sustainable Cities and Society 45:38-47.

[27] Rehman S, Mohandes M (2008) Artificial neural network estimation of global solar radiation using air temperature and relative humidity. Energy Policy 36:571-576.

[28] Behar O, Sbarbaro D, Marzo A, Moran L (2019) A simplified methodology to estimate solar irradiance and atmospheric turbidity from ambient temperature and relative humidity. Renewable and Sustainable Energy Reviews 116:109310.

[29] Ziarani NN, Haghighi AP (2019) Anticipating an efficient relative humidity in a room under direct solar radiation and equipped by radiant cooling panel systemAnticiper une humidité relative efficace dans une pièce exposée au rayonnement solaire direct et équipée d'un système de refroidissement par panneaux rayonnants. International Journal of Refrigeration 98 :98-108.

[30] Woolley J, Schiavon S, Bauman F, Raftery P (2019) Side-by-side laboratory comparison of radiant and all-air cooling: How natural ventilation cooling and heat gain characteristics impact space heat extraction rates and daily thermal energy use. Energy and Buildings 200:68-85.

[31] Magalhães F, Moura FCC, Lago RM (2011) TiO_2/LDPE composites: A new floating photocatalyst for solar degradation of organic contaminants. Desalination 276:266-271.

[32] Tsumura T, Hattori Y, Kaneko K, Hirose Y, Inagaki M, Toyoda M (2004) Formation of the Ti_4O_7 phase through interaction between coated carbon and TiO_2. Desalination 169:269-275.

[33] Relinque EJ, Castellote M (2018) Hydroxyl radical and free and shallowly trapped electron generation and electron/hole recombination rates in TiO_2 photocatalysis using different combinations of anatase and rutile. Applied Catalysis A: General 565:20-25.

[34] Choi H, Stathatos E, Dionysiou DD (2007) Photocatalytic TiO_2 films and membranes for the development of efficient wastewater treatment and reuse systems. Desalination 202:199-206.

[35] Kitazawa S, Choi Y, Yamamoto S, Yamaki T (2006) Rutile and anatase mixed crystal TiO_2 thin films prepared by pulsed laser deposition. Thin Solid Films 515:1901-1904.

[36] Eufinger K, Poelman D, Poelman H, De Gryse R, Marin GB (2007) Effect of microstructure and crystallinity on the photocatalytic activity of TiO_2 thin films deposited by dc magnetron sputtering. Journal of Physics D: Applied Physics 40:5232-5238.

[37] Komaraiah D, Radha E, Sivakumar J, Ramana Reddy MV, Sayanna R (2019) Structural, optical properties and photocatalytic activity of Fe^{3+} doped TiO_2 thin films deposited by sol-gel spin coating. Surfaces and Interfaces 17 (2019) 100368.

[38] Malengreaux CM, Léonard GML, Pirard SL, Cimieri I, Lambert SD, Bartlett JR, Heinrichs B (2014) How to modify the photocatalytic activity of TiO_2 thin films through their roughness by using additives. A relation between kinetics, morphology and synthesis. Chemical Engineering Journal 243: 537-548.

[39] Abdelkrim A, Rahmane S, Abdelouahab O, Hafida A, Nabila K (2016) Optoelectronic properties of SnO_2 thin films sprayed at different deposition times. Chinese Phys. B 25:046801.

[40] Tauc J, Menth A (1972) States in the gap. J. Non-Cryst Solids 8-10:569-585.

[41] Rahmane S, Aida MS, Djouadi MA, Barreau N (2015) Effects of Thickness Variation on Properties of ZnO:Al Thin Films Grown by RF Magnetron Sputtering Deposition. Superlattices and Microstructures 79:148-155.

[42] Zhang D, Zhang M, Chen S, Liang Q, Sheng N, Han Z, Cai Y, Wang H (2021) Scalable, self-cleaning and self-floating bi-layered bacterial cellulose biofoam for efficient solar evaporator with photocatalytic purification. Desalination 500:114899.

[43] Zayani G, Bousselmi L, Mhenni F, Ghrabi A (2009) Solar photocatalytic degradation of commercial textile azo dyes: Performance of pilot plant scale thin film fixed-bed reactor. Desalination 246:344-352.

[44] Mahvi AH, Ghanbarian M, Nasseri S, Khairi A (2009) Mineralization and discoloration of textile wastewater by TiO_2 nanoparticles. Desalination 239:309–316.

[45] Wang J, Ma T, Zhang Z, Zhang X, Jiang Y, Pan Z, Wen F, Kang P, Zhang P (2006) Investigation on the sonocatalytic degradation of methyl orange in the presence of nanometer anatase and rutile TiO_2 powders and comparison of their sonocatalytic activities. Desalination 195:294–305.

[46] Bharti B, Kumar S, Kumar R (2016) Superhydrophilic TiO_2 thin film by nanometer scale surface roughness and dangling bonds. Applied Surface Science 364:51-60.

[47] Begum NS, Ahmed HMF, Gunashekar KR (2008) Effects of Ni doping on photocatalytic activity of TiO_2 thin films prepared by liquid phase deposition technique. Bull. Mater. Sci. 31:747–751.

[48] Kim H, Gilmore CM (1999) Electrical, optical, and structural properties of indium–tin–oxide thin films for organic light-emitting devices. J. Appl. Phys. 86:6451-6461.

[49] Bansode AS, More S, Bhoraskar SV, Mathe VL (2015) Reusable thin film photocatalyst of Fe-doped TiO_2 deposited by ECR plasma, surface and interface analysis 47:22-29.

Figures

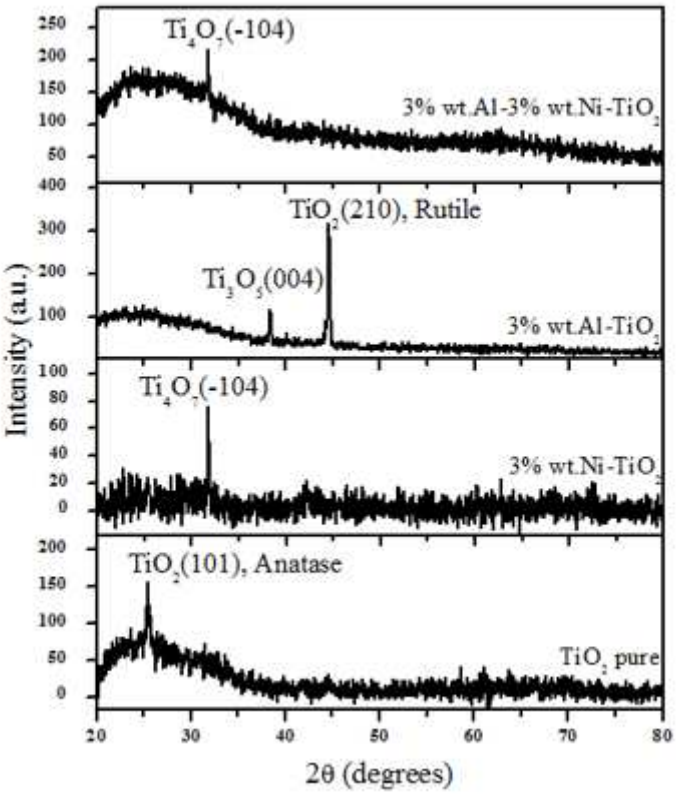

Figure 1

XRD patterns of TiO2 based thin films.

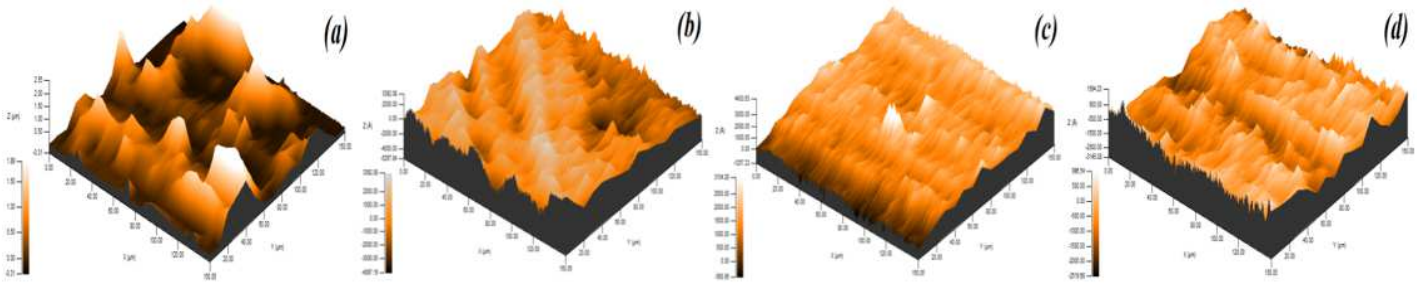

Figure 2

3D surface topography of TiO2 based thin films: (a) TiO2 pure, (b) 3 wt. %Ni-TiO2, (c) 3 wt. %Al-TiO2, (d) 3 wt. %Ni-3 wt. %Al-TiO2.

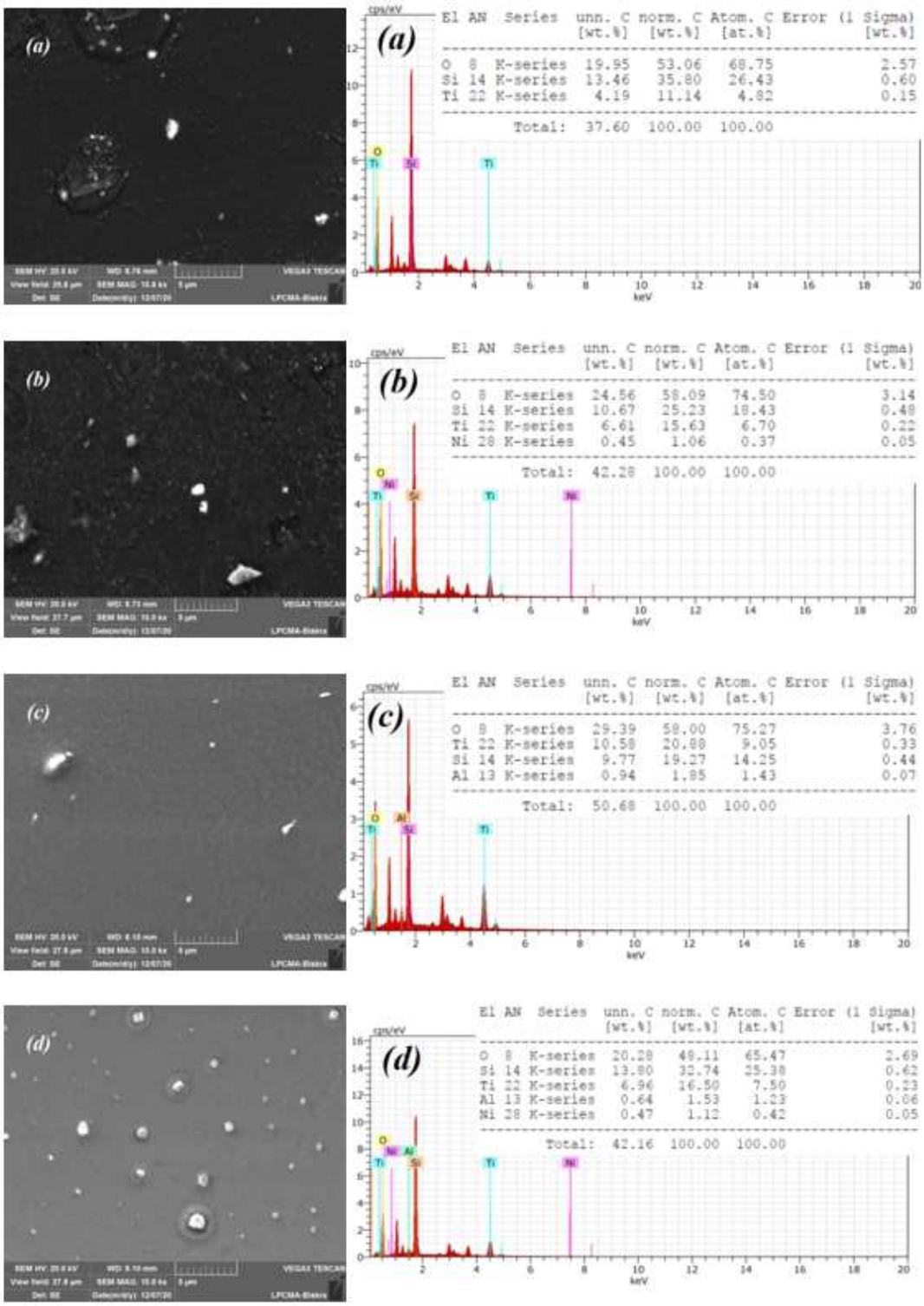

Figure 3

SEM and EDX analyses of TiO2 based thin films: (a) TiO2 pure, (b) 3 wt. %Ni-TiO2, (c) 3 wt. %Al-TiO2, (d) 3 wt. %Ni-3 wt. %Al-TiO2.

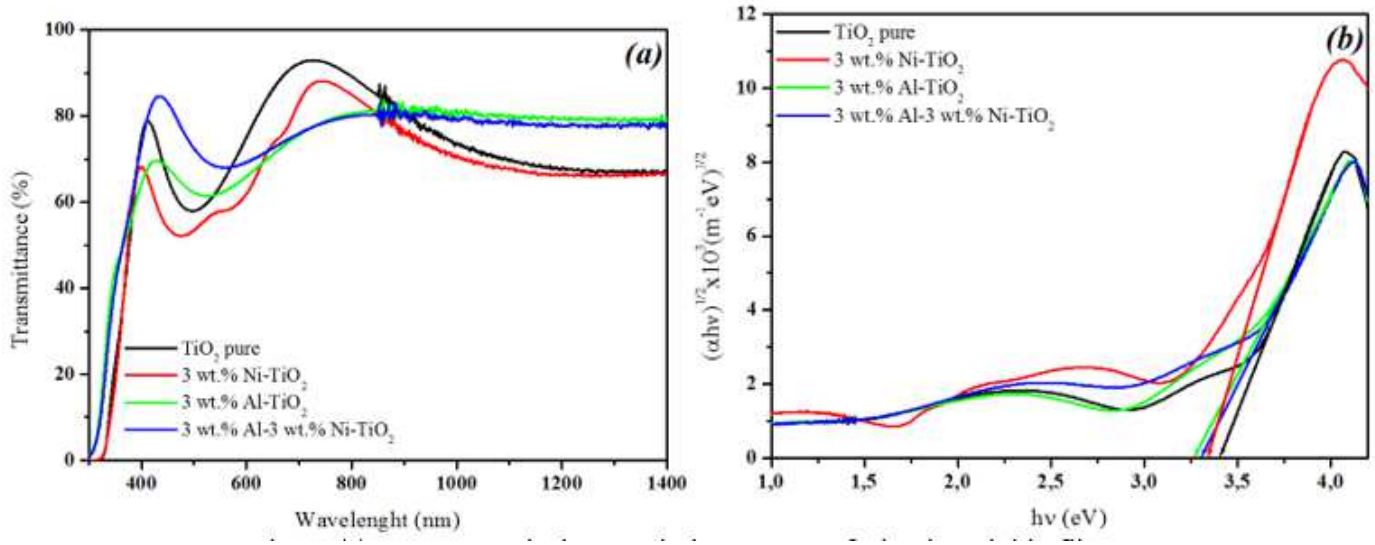

Figure 4

(a) UV-VIS optical transmission spectra of TiO2 based thin films, (b) Tauc plot for the optical band gap.

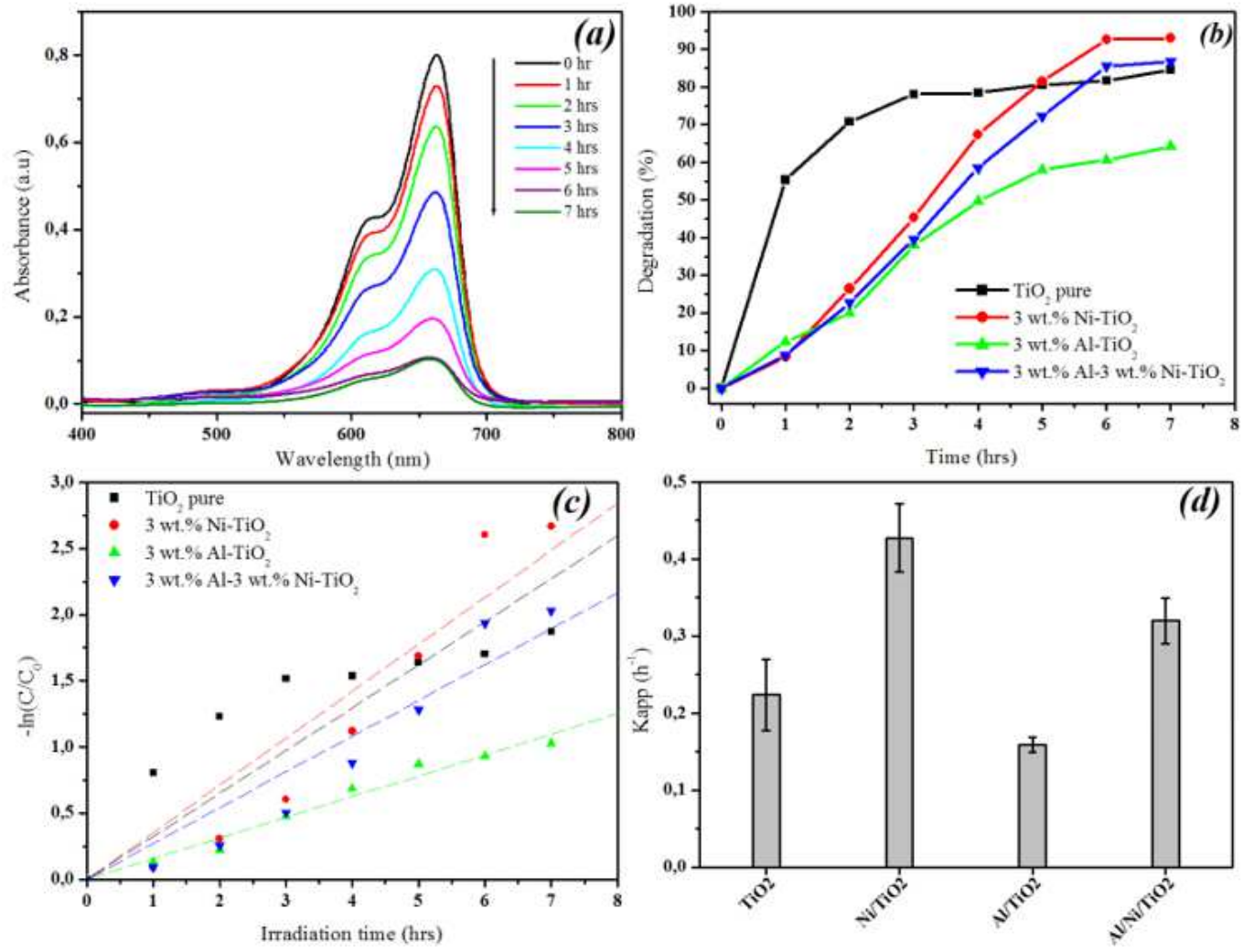

Figure 5

(a) Variation of UV–vis spectra of MB during photodegradation over Ni/TiO2 thin films; (b) Plot of photocatalytic efficiency versus the degradation time; (c) plot of ln (C/C0) versus irradiation time for TiO2 based films; (d) rate constant k of MB photodegradation.

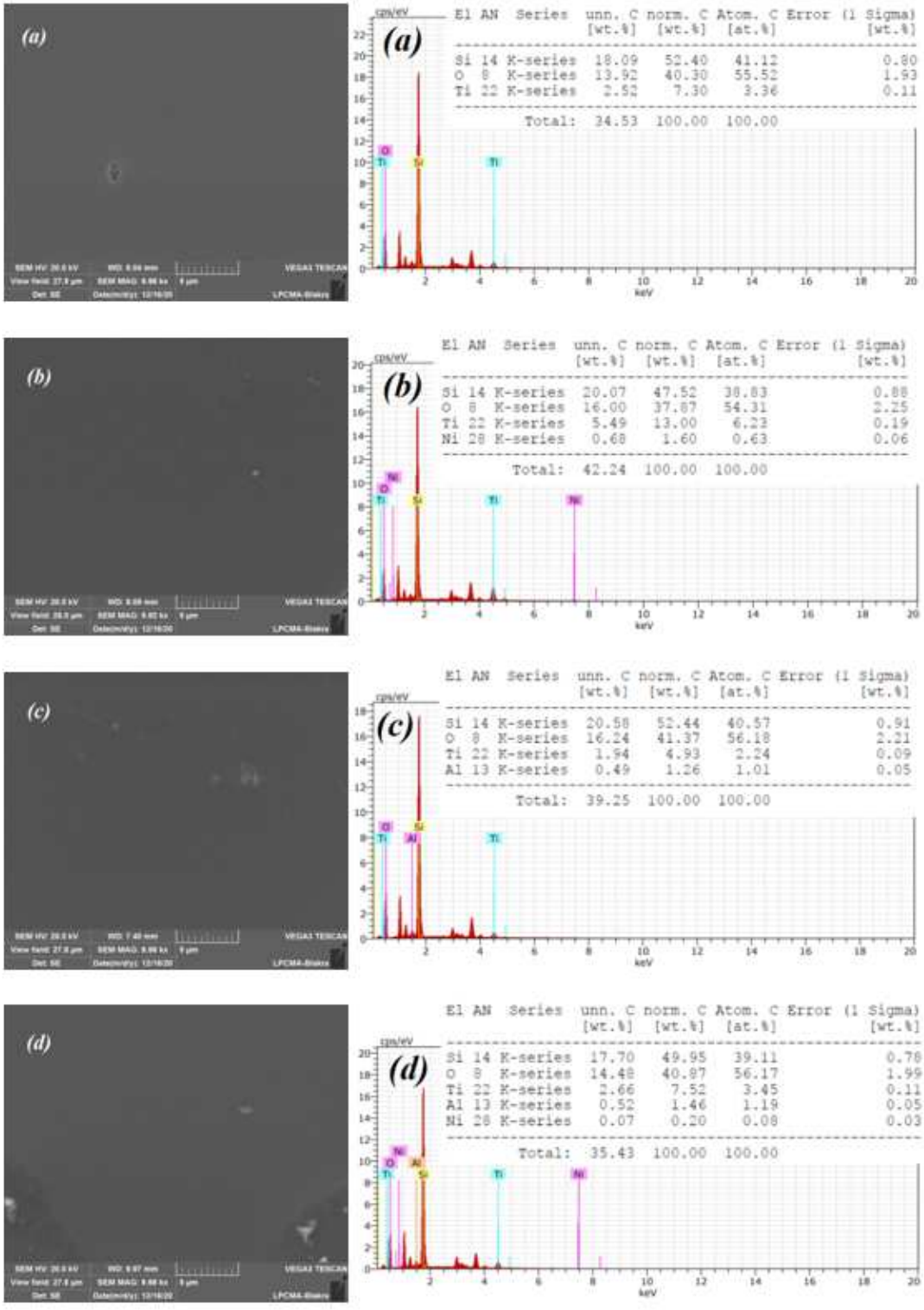

Figure 6

SEM and EDX analyses of TiO2 based thin films after photodegradation process: (a) TiO2 pure, (b) 3 wt. %Ni-TiO2, (c) 3 wt. %Al-TiO2, (d) 3 wt. % Al-3 wt. % Ni-TiO2.

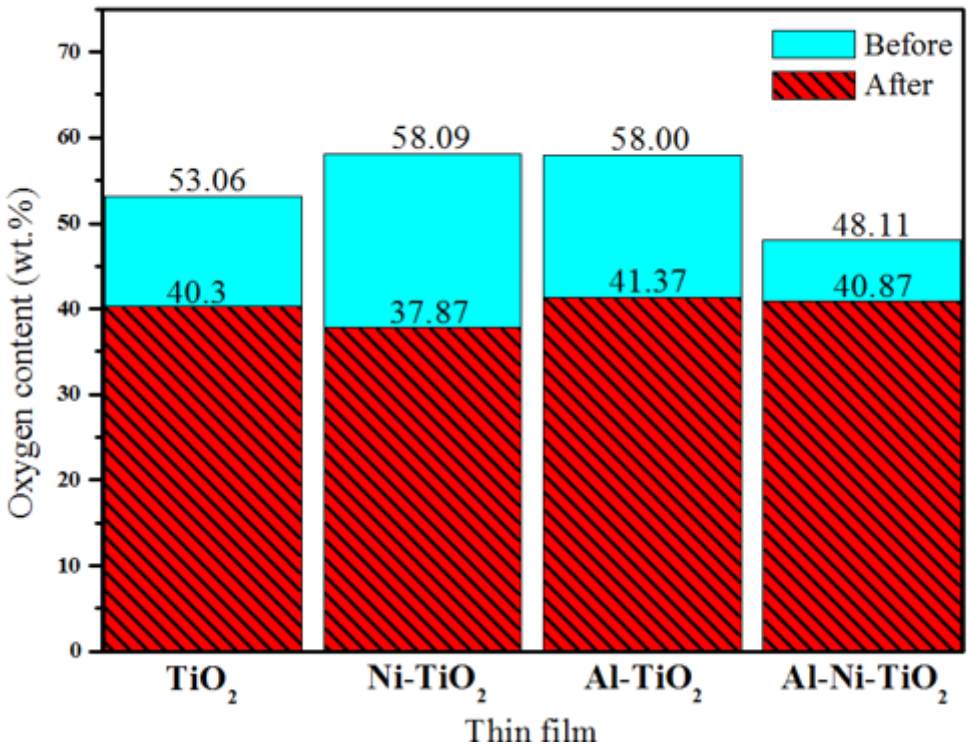

Figure 7

Effect of photocatalysis process on oxygen content in the films.

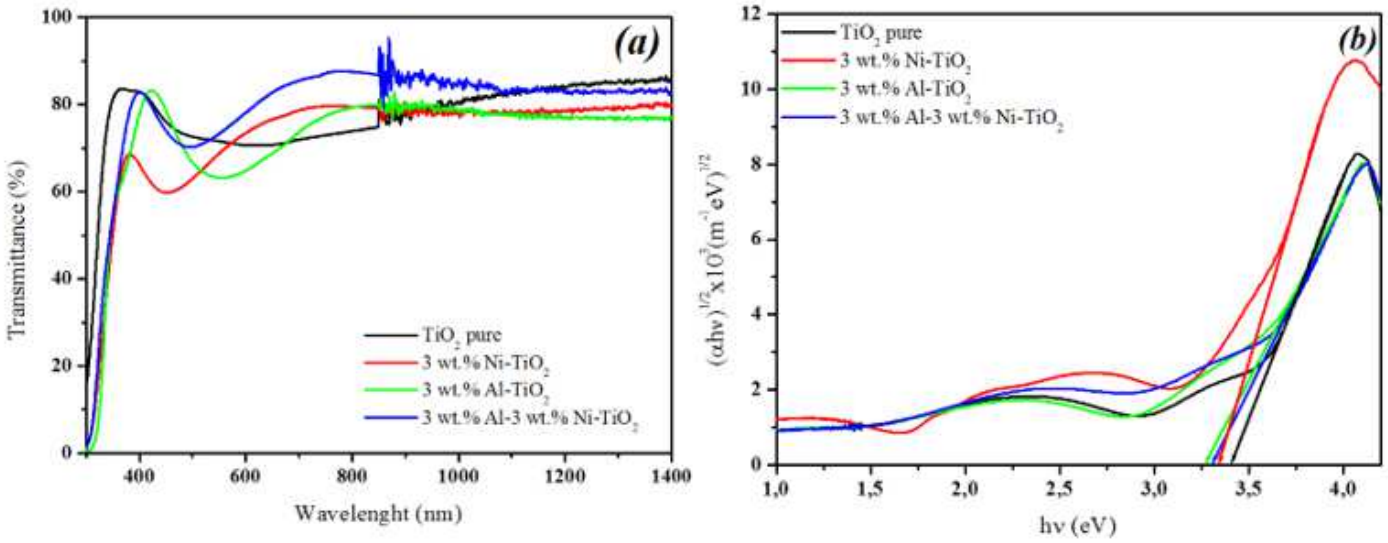

Figure 8

(a) UV-VIS optical transmission spectra of TiO2 based thin films after photodegradation process, (b) Tauc plot for the optical band gap.

Supplementary Files

This is a list of supplementary files associated with this preprint. Click to download.

- Anatase.tif